Thin Solid Films 517 (2009) 1949–1957

Contents lists available at ScienceDirect

Thin Solid Films

journal homepage: www.elsevier.com/locate/tsf

Kinetic Monte Carlo simulation of an atomistic model for oxide island formation and step pinning during etching by oxygen of vicinal Si(100)

Marvin A. Albao [a], Feng-Chuan Chuang [a,*], J.W. Evans [b,c]

[a] Department of Physics, National Sun Yat-Sen University, Kaohsiung, 804, Taiwan
[b] Ames Laboratory-USDOE, Iowa State University, Ames, IA 50011, USA
[c] Department of Mathematics, Iowa State University, Ames, IA 50011, USA

ARTICLE INFO

Article history:
Received 21 December 2007
Received in revised form 3 September 2008
Accepted 19 October 2008
Available online 5 November 2008

Keywords:
Si oxidation
Thin film growth
Kinetic Monte Carlo simulation
Etching
Nucleation

ABSTRACT

A lattice-gas model is developed to describe the simultaneous oxidation and etching of Si(100) surfaces exposed oxygen. The model incorporates nucleation of oxide islands via conversion of on-surface to back-bonded oxygen, together with an observed transformation in the shapes of just-formed islands from linear to two-dimensional. Model analysis via Kinetic Monte Carlo simulation quantifies oxygen uptake and oxide island nucleation kinetics, including possible enhanced nucleation at step edges. Simulated etching of vicinal Si(100) surfaces reveals that receding steps are pinned by oxide islands and transform into finger-like structures even at higher temperatures where oxide island growth is inhibited.

1. Introduction

In the fabrication of semiconductor devices, a trend towards miniaturization increasingly relies on more nuanced understanding of the surface roughening. This roughening process is an inevitable byproduct of even the briefest exposure of silicon surfaces to oxygen. Such an understanding allows for greater control and consistency in the fabrication of high-quality integrated circuit components and other devices that are the staple of the microelectronics industry.

Thus, a key goal has been to develop atomistic models for etching and oxidation of silicon surfaces [1–3] in which the key competitive processes are $Si+1/2O_2(gas) \rightarrow SiO(gas)+vacancy$ [etching] and $Si+O_2(gas) \rightarrow SiO_2$ [oxidation]. Vacancies created by the first process lead to etching, whereas oxide islands formed by the second process mask the underlying Si from etching. The modeling should cut across a broad range of conditions, from the regime of rapid oxide growth at low temperature and/or high oxygen pressure, to an etching-dominated regime at high-temperature and/or low pressure. The challenge is to accurately describe the evolution of the far-from-equilibrium surface morphology including: etch pit formation and step recession on vicinal surfaces at higher temperature; the formation of oxide islands and associated step pinning; and the ultimate emergence of oxide-covered Si nano-protusions at moderate temperature [1,4–6].

However, such modeling has been hampered by lack of information on the details of oxide island nucleation process under the appropriate ultra-high-vacuum conditions. Access to and incorporation of more detailed information on this nucleation process and on oxide island structure would allow more reliable modeling of oxygen surface dynamics (oxygen uptake, oxide nucleation, and SiO desorption kinetics) as well as of surface morphology. It would also facilitate determination of associated energetics by comparison of model predictions with experiment.

Recent ultra-high-vacuum experimental Scanning Tunneling Microscopy (STM) studies by Togashi et al. [7] and an earlier work by Udegawa and coworkers [8] together with theoretical electronic structure studies [9] suggest a detailed picture for the nucleation and growth of surface oxide islands during exposure of Si(100)−2×1 surfaces to molecular oxygen at around 600 °C. STM studies performed at 560 °C reveal the initial formation of linear islands of back-bonded oxygen with length up to 4 atoms (apparently orthogonal to the Si dimer rows) followed by a transition to small two-dimensional (2D) compact islands. Small two-dimensional islands with odd sizes (of 3 and 5) are rarely seen suggesting that the kink sites on these islands are favorable attachment sites so that these islands have short lifetimes.

In addition, embedded-cluster quantum chemistry calculations using the Surface Integrated Molecular Orbital/Molecular Mechanics (SIMOMM) approach [10] indicate three strongly-bonded surface oxygen species. Furthermore, two of these (on-dimer and dimer-bridge, where the latter is slightly more strongly bonded) can readily interconvert. Thus, we can effectively treat them as a single on-surface (OS) oxygen species. Of particular significance is the SIMOMM prediction that an isolated OS oxygen can convert to the third

* Corresponding author. Tel.: +886 7 5253733; fax: +886 7 5253709.
E-mail address: fchuang@mail.nsysu.edu.tw (F.-C. Chuang).

0040-6090/$ – see front matter © 2008 Elsevier B.V. All rights reserved.
doi:10.1016/j.tsf.2008.10.055

strongly-bonded sub-surface back-bonded (BB) oxygen species which has roughly the same energy as the OS species. However, there is a substantial barrier, E_{con} ~3.0–3.3 eV for OS to BB conversion, and thus an equal barrier of E_{con} for reconversion.

Previous work also revealed an apparent weak link between oxide island population and the density of steps. This issue was the main focus of a prior study by Brichzin and co-workers [11] aimed at exploring the impact of high surface step density on the nucleation rate for oxide islands, the etching rate, and the oxygen sticking probability. Along with an observed increase in the sticking coefficient in regions with high step density, these authors concluded that an as yet undetermined mechanism for enhancing oxide nucleation rate (perhaps involving a lowering of the nucleation barriers at or near the steps) could account for the observed phenomenon. This view is consistent with the earlier findings of Wei et al. [12], in which a steady increase in nucleation activity was observed in Si(100) with progressively higher miscut angles relative to the flat terrace. A more recent electronic structure study [13] on adsorption of oxygen on Si(100) steps likewise arrived at a similar conclusion, namely that there is preferential adsorption on step edges which is both elastic and electronic in origin. Furthermore, Mazzone et al. noted that so-called S_B steps (following Chadi's nomenclature [14]) act as better traps for O monomers than S_A steps, echoing the prediction by Brichzin, et al. in Ref. [11].

Together, these observations help build a refined atomistic model incorporating a more realistic oxide island nucleation and growth mechanism. The model should be capable of describing the details of island sizes and shapes observed by STM at 560 °C, but also applicable to other temperature regimes. Just as for the models developed previously [1–3], the new model should be able to describe oxygen uptake dynamics [15] and oxide island nucleation kinetics quantified in previous experimental studies [4–6]. It might also assess propensity of oxide islands to pin receding steps during etching of vicinal Si(100), particularly at higher temperatures where island growth is inhibited so that the initial island shape are more relevant. In addition, the new model should enable exploration of possible links between oxide island population and step density.

This paper is organized as follows. The key studies and open challenges which motivated and guided the current work are reviewed above in Section 1. In the following Section 2, we provide a detailed description of the atomistic lattice-gas model which we apply to explore various issues associated with etching and oxidation. This model was constructed to incorporate a more realistic oxide island nucleation mechanism and to reproduce experimental observations of shape transitions in oxide island growth. In Section 3, we first present Kinetic Monte Carlo (KMC) simulation results illustrating the behavior of oxide island shapes, and then show that model predictions for oxygen uptake and oxide island density with realistic choices for energetic parameters are reasonably consistent with experimental data. Some analytic interpretation of behavior is also provided. Then, we explore one candidate mechanism for enhanced oxide cluster nucleation at the steps. We close this section by examining the effectiveness of small oxide islands on step pinning and the development of finger morphologies at higher temperature, including an assessment of the effect of initial island shape. Finally, we provide concluding remarks in Section 4.

2. Atomistic lattice-gas modeling

In describing atomistic processes relevant to etching and oxidation of Si(100) surfaces, it is instructive to distinguish processes involving oxygen (adsorption, dissociation, diffusion, etching by formation of volatile SiO, and oxide island nucleation) from those pertaining specifically to silicon surface dynamics. Below, we first focus on processes related to oxygen dynamics, emphasizing key features incorporated for the first time into the current modeling. We then discuss briefly the treatment of silicon surface dynamics noting that for the latter, we adopt exactly the same formulation as in our previous modeling [3]. Rates for all thermally activated process are assumed to have an Arrhenius form, $h = \nu exp[-E_{act}/(kT)]$ where E_{act} denotes the activation energy, and ν the prefactor.

For the *oxygen dynamics*, a key feature in our modeling is the distinction between two types of strongly-bonded surface oxygen species involved during oxidation, namely, on-surface (OS) and back-bonded (BB) species. For simplicity, both OS and BB species are treated as being located on a common square lattice of sites, and their dynamics is modeled within an atomistic lattice-gas model framework. We shall ignore all interactions between OS oxygen, and include only nearest-neighbor (NN) pairwise attractions of strength E_{ox} between BB oxygen. These latter interactions drive the formation and stabilization of oxide clusters.

The following are the key processes involving oxygen:

(i) *Dissociative adsorption*. Molecular oxygen adsorbs dissociatively on neighboring empty sites creating adjacent pairs of OS atoms.

(ii) *Surface Diffusion*. In the simplest scenario adopted here, only the OS atoms are mobile on the surface. Their diffusion barrier was previously estimated at E_O ~2.0–2.5 eV [16]. OS oxygen can "quickly" hop to any NN site provided that site is free of other species and does not coincide with a BB oxygen. (Thus, adjacent pairs of OS oxygen created by dissociative adsorption typically separate immediately via surface diffusion.)

(iii) *Creation of linear oxide clusters*. Isolated OS oxygen converts to BB species with barrier E_{con}. To induce formation of linear oxide islands or chains, we impose a reduced barrier of $E_{con}-c_1E_{ox}$ for conversion of OS oxygen if located on a suitable NN site of an isolated BB O to initiate formation of a linear chain of BB O with the appropriate orientation (orthogonal to surface Si dimer rows). The same reduced barrier applies for conversion of OS oxygen located on a NN site at the end of a linear chain of length 2 or 3. There is no significant population of linear chains of length greater than 4 suggesting that strain effects eliminate enhanced exchange for longer chains. Thus, it is not included in our modeling. By detailed-balance, the barrier to reconvert to OS oxygen from the end of a linear BB chain of length 2, 3, or 4 is given by $E_{con}+(1-c_1)E_{ox}$.

(iv) *Development of 2D oxide clusters*. One could also introduce enhanced conversion at perimeter sites of BB clusters with the degree of enhancement depending on the local configuration. Such enhancement would be weaker for sites along the sides of short linear islands (since such islands dominate over small 2D islands), and stronger at doubly-coordinated kink sites (as one does not observe a significant population of bent trimers or 5-atom islands with kink site). Specifically, we assume enhanced conversion at kink sites with barrier $E_{con}-c_2E_{ox}$, selecting $c_2>c_1$. Accounting for detailed-balance, we must then impose a barrier of $E_{con}+(2-c_2)E_{ox}$ for the reverse process since such exchanged O are doubly-bonded in the oxide island. For triply-coordinated "double-kink" sites, conversion is similarly enhanced, with barrier $E_{con}-c_3E_{ox}$, choosing $c_3>c_2$. For the reverse process, a high barrier of $E_{con}+(3-c_3)E_{ox}$ is imposed. In Fig. 1, we present a schematic illustrating the different configurations described here.

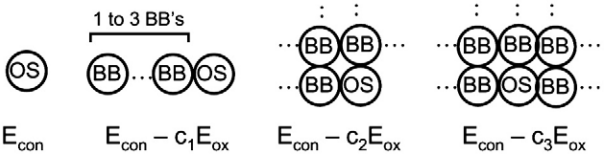

Fig. 1. Schematic of configurations relevant for conversion of OS to BB oxygen, together with the corresponding barriers.

(v) *Desorption of SiO*. OS oxygen can desorb with barrier E_{des} as SiO by removing the Si on the site directly beneath the oxygen to create a surface vacancy. OS oxygen can also react with adjacent isolated Si adatoms with the same barrier.

As an aside, we note that in the following section, we will introduce some refinements to the above prescription of oxygen surface dynamics near step edges which are designed to produce enhanced oxide formation at these locations.

Next, we briefly discuss the most important features of our treatment of the *silicon surface dynamics*. The etching process, $Si+1/2O_2(gas)\rightarrow SiO(gas)$, creates single vacancies (SV) on the Si(100) surface. These are believed to immediately convert to more stable di-vacancies (DV) by ejecting an unpaired Si up onto the surface. Both the Si adatoms and the DV exhibit strongly anisotropic surface diffusion preferring the dimer row direction. Si adatoms diffuse across terraces and attach to S_B steps producing some step growth (and rarely pairs of adatoms can recombine to form Si ad-dimers). However, this process is dominated by DV's diffusing to such steps and producing step erosion. Under certain conditions, these DVs can also aggregate to nucleate etch pits on terraces. It should also be emphasized that Si(100) surfaces, particularly vicinal surfaces, are highly dynamic even in the absence of exposure to oxygen. Si-dimers continually detach and reattach from step edges subject to strongly anisotropic step energetics (with stronger interactions along dimer rows versus across them). The feature that the dimer rows alternate direction on consecutive terraces, together with the anisotropy in Si dimer interaction, produces the well-known feature of alternating rough S_B steps and straight S_A steps on vicinal surfaces. Our modeling includes all of these features within an atomistic lattice-gas model framework, details of which were described in our previous work [3].

Our KMC simulations of the above lattice-gas model use a Bortz–Kalos–Lebowitz (BKL) type algorithm [17] which is based on the creation of dynamically updated lists of adspecies grouped according to those undergoing processes with similar rates. This BKL type algorithm avoids high-rejection rates of standard algorithms in that at any given Monte Carlo step, some process is quite likely to be implemented. (A finite probability of failure derives from the feature that our lists include particles undergoing processes with some spread in rates, so those with slower rates are accepted with probability somewhat less than one.) Thus, BKL efficiency derives from the fact that every Monte Carlo step is likely to advance the system along its evolutionary path.

Next, we offer a few additional remarks on parameter selection. The oxygen adsorption rate, F, reported in monolayers (ML)/sec, is always assigned the appropriate experimental value. Based on previous experiments [15], this is related to the oxygen pressure (in Torr) by $F=2.7\times10^4\ P_{O2}$. For the rates of thermally activated processes, the choice of activation barriers and the corresponding prefactors, is often guided by previous results from experiments or first-principles calculations, as well as from KMC studies. These are summarized in Table 1. While these sources are useful in providing initial estimates for certain key parameters, our own simulations can often narrow down the range of acceptable values or rule out certain choices. Ideally, the model with a single standard or universal set of parameters should be able to describe all experimental observations. However, the sheer diversity of experiments (STM analysis of small oxide islands, analysis of oxygen uptake and oxide island densities, STM characterization pinned step morphologies), and the broad range of conditions under which they were performed, means that perfect universal agreement of model and experiment is unlikely. Also, some input parameters taken from previous studies are undoubtedly effective values geared to certain narrow ranges of conditions. This feature, together with uncertainties concerning the atomistic details of various processes in these complex systems means some discrepancies should be expected. We do identify a standard set of parameters which can reasonably describe key observations of small oxide island structure, oxygen uptake, and step pinning, sometimes with small refinements in energies to enhance agreement. There is a larger discrepancy in predicting oxide island densities (perhaps due to uncertainties of atomistic details of the nucleation process), on which we comment below.

Finally, we note that in the above model, and in the physical etching and oxidation process, there is weak coupling of the oxygen surface dynamics to the underlying silicon surface dynamics. (However, the coupling in the reverse direction is strong, i.e., oxide island formation greatly impacts the morphological evolution of the etched surface.) Our prescription of dissociative adsorption of oxygen to form OS species, OS oxygen diffusion, conversion to and reconversion from BB oxygen, and removal of oxygen from the surface via desorption as SiO, does not depend on the local surface morphology. Thus, the only coupling of the oxygen to the silicon surface dynamics comes from rare reaction with Si adatoms, and from modifications to the model described in Section 3.5 designed to enhance oxide island formation at step edges. Consequently, from the perspective of analysis of oxygen surface dynamics, it is natural to consider a *simplified model* where one completely ignores the coupling of processes involving oxygen to the Si surface dynamics. Here, removal of oxygen via SiO desorption (producing etching in the physical system and in the full model) is replaced by non-associative desorption of atomic oxygen in the simplified model. In both cases, one oxygen atom is removed from the surface, but the simplified model ignores the feature that this oxygen atom takes with it a Si atom from the surface creating a vacancy. The value of the simplified model is that one can perform a more efficient simulation analysis of the dependence of oxygen surface dynamics (e.g., oxygen uptake, and oxide island nucleation) on model parameters than in the full model.

Table 1
Energies and prefactors used in the atomistic lattice-gas model

Process	Notation	Barrier (eV)	Prefactor (per second)
OS to BB conversion	E_{con}	3.04±0.04 [a]	10^{16} [d]
SiO Desorption	E_{des}	3.5±0.1 [b]	4×10^{19} [e]
O diffusion	E_O	2.45±0.05 [c]	10^{16} [f]
BB NN interaction	E_{ox}	1.2	

[a]Based on SIMOMM calculations in Ref.[10].
[b]SIMOMM estimate in Ref. [10] is close to 4 eV, higher than the 3.8 eV prediction of a GGA study (see Ref. [18]); KMC simulation studies in Refs. [2,3] suggest far lower values [3.2–3.5 eV] consistent with those reported in Ref. [19].
[c]DFT studies in Ref. [16] suggest a value within the [2.0–2.5 eV] range. KMC simulations Refs. [1–3] likewise adopted values within the narrow range [2.4–2.5 eV].
[d]Simulations of oxide island density used a lower prefactor of $10^{13.5}\ s^{-1}$ as discussed in the text.
[e]Adopted from Ref. [19].
[f]Adopted from Refs. [1–3].
Values reported correspond to our "standard" choice used to successfully describe shapes and sizes of small oxide islands. In other analyses, small changes are sometimes made in activation barriers, and the range of variation is indicated. Prefactors are not varied with one exception which is noted. We use values of $c_1=0.2$, $c_2=0.4$, $c_3=0.5$, to describe enhanced OS to BB conversion.

3. Results and discussion

3.1. Transformation of initial oxide cluster shape

Our goal here is to demonstrate that with an appropriate choice of kinetic parameters, the model described in Section 2 can replicate the qualitative features observed experimentally by Togashi et al. as detailed in Ref. [7]. Specifically, the model should produce a shape transformation in oxide islands from linear to two-dimensional forms as the size increases. This feature is characterized quantitatively by the population distributions for linear and 2D islands of various sizes. In Fig. 2, we compare experimental STM data from Ref. [7] with simulation results for an ensemble of oxide islands as predicted by

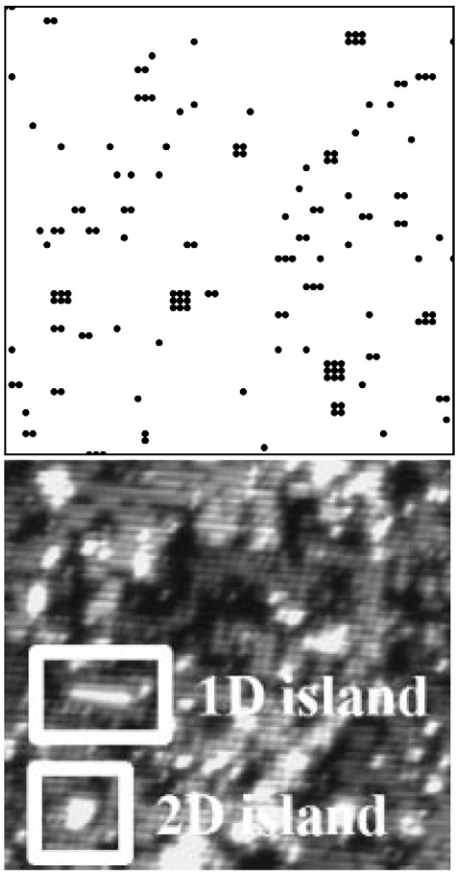

Fig. 2. *(Top)* Simulation results for an ensemble of oxide islands at 560 °C and F=0.0136 ML/s showing 0.035 ML BB oxide coverage. Area: 35 nm×35 nm. *(Bottom)* STM image from Ref. [7] showing oxide islands as bright spots at 560 °C and oxygen pressure of 5×10^{-7} Torr. Area: 35 nm×35 nm.

the simplified model at 560 °C with a pressure of 5×10^{-7} Torr. We choose E_{des}=3.5 eV and E_{con}=3.04 eV (our standard choice of parameters). In the simulations, the oxygen pressure is equivalent to F=0.0136 ML/s, while the final coverage of BB atoms is roughly 0.035 ML and is chosen to coincide with the oxide island coverage in the experiments. Coexistence between linear and 2D islands is evident. The corresponding population distributions are shown in Fig. 3. The predictions in the simulation plots capture the general trend observed in the experiments in which linear islands dominate for smaller sizes $s<4$, but 2D islands become more abundant starting at $s=4$. Simulations also reveal a relative scarcity of odd-number island sizes ($s=3,5$), compared with even-number ones ($s=4,6$), again consistent with experiments. The authors in the experimental study attributed this to the feature that kink sites in odd-number islands are easily "filled" by migrating oxygen species. Here, we emphasize that the island distributions described above are characteristic only of short-time exposure to oxygen. The development of "mature" shapes for longer times and the ramifications for oxygen uptake kinetics will be discussed below.

3.2. Review of experiments and theories for oxygen uptake and oxide nucleation kinetics

Suemitsu et al. [15] investigated the oxygen uptake kinetics measured from real-time ultraviolet photoelectron spectroscopy (UPS). The key observation is that the oxygen coverage, θ_O, versus time has a sigmoidal form for higher temperatures or lower oxygen pressures, i.e., initial inhibition or slow uptake, followed by an "autocatalytic increase", and finally saturation. This sigmoidal form converts to a Langmuir form for lower temperatures or higher oxygen pressures. Pelz and coworkers [1,4–6,11] performed numerous STM studies, as well as one simulation analyses, of oxide island nucleation on Si(100). We shall describe some of their results below.

It is instructive at this point to review various analytic formulations for this behavior before discussing our simulation results, particularly since such reviews are lacking in the literature:

(i) The heuristic autocatalytic rate (ACR) model [15] adopts a rate equation description of uptake kinetics, $d\theta_O/dt\approx(1-\theta_O)(\theta_O+\theta^*)/\theta^*$ where θ^* denotes the coverage at which island formation commences. Large (small) θ^* describes Langmuir (sigmoidal) kinetics. The ACR model was quite successful in fitting experimental data. For sigmoidal kinetics (corresponding to inhibition of oxide island nucleation) with θ_O significantly above small θ^*, one has that $d\theta_O/dt\approx(1-\theta_O)(\theta_O+\theta^*)$, which peaks at $\theta_O=1/2$. The right hand side might be regarded as (proportional to) a rough measure of the perimeter length of oxide islands.

(ii) A simple atomistic model recovering the above kinetics includes random deposition and desorption, diffusion of deposited species and irreversible aggregation into islands [20,21]. Negligible (high) desorption rate yields Langmuir (sigmoidal) kinetics as confirmed by simulations. It has been noted [20] that this model corresponds to what is called "incomplete condensation" with irreversible island formation (critical size $i=1$) in the literature on island nucleation during deposition on surfaces [22,23]. The above general features of the kinetics are preserved if one generalizes the above model to allow reversible island formation [20] corresponding to "incomplete condensation" with critical size $i>1$ [22,23].

(iii) It is straightforward to see that "incomplete condensation" models with large desorption rates (i.e., in the regime of sigmoidal

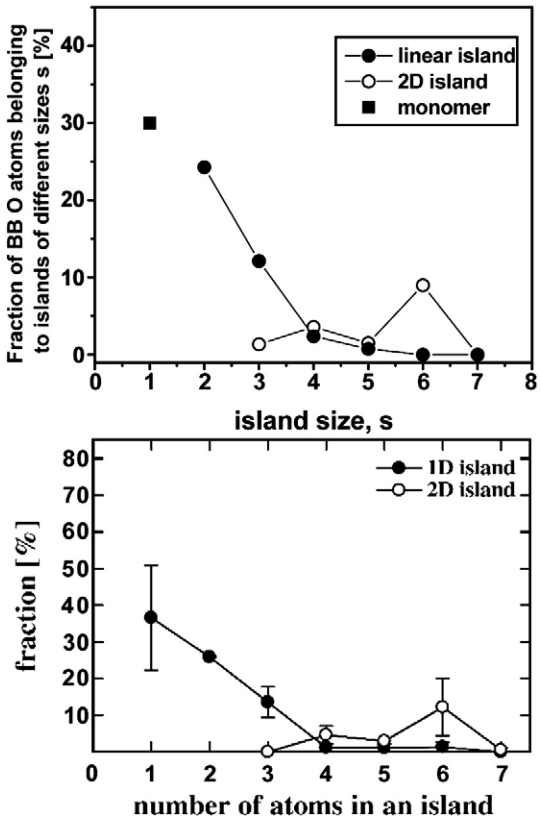

Fig. 3. *(Top)* Simulation plot of fraction of BB atoms belonging to an oxide island of size s versus s. Operating conditions in the simulation is the same as in Fig. 2. *(Bottom)* Experimental plot from Ref. [7] showing fraction of BB atoms belonging to an oxide island of size s versus s.

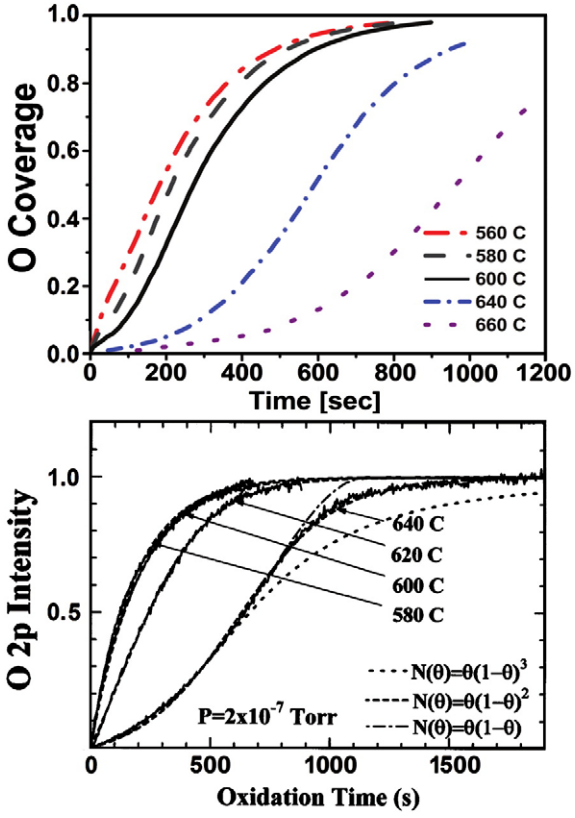

Fig. 4. *(Top)* Simulation of oxygen uptake curves for temperatures 560, 580, 600, 640 and 660 °C (left to right) and fixed pressure 2×10^{-7} Torr. *(Bottom)* O 2p UPS intensity vs oxidation time plot from Ref. [15] shows oxygen uptake behavior for temperatures 580, 600, 620 and 640 °C at fixed pressure of 2×10^{-7} Torr. Reprinted with permission from Ref. [15]. Copyright 1998 by the American Physical Society.

kinetics) reduce to so-called Avrami models [22,24–27]. In this regime, the diffusion length, L_{diff}, of adspecies (before desorption) is far below the island separation. Thus, aggregation with island edges only occurs for atoms deposited in a ring within a short distance of the perimeter. Consequently, the island perimeter expands with roughly constant velocity, v. Since the adspecies density is uniform at distances greater than L_{diff} island edges, nucleation occurs at random locations on the surface at rate I, say. These are the two ingredients of the classic Avrami model [24–26] which provides a canonical realization of sigmoidal kinetics (see below).

(iv) Generalized Avrami models [28,29] incorporate random nucleation of islands at rate I, but allow for the possibility that the expansion velocity, $v(\tau)$, of the island radius depends on the time since nucleation, τ. Equivalently, one can consider the expansion velocity depending on the island radius or dimension. One can obtain the exact expression for the uptake kinetics of the form [28].

$$1-\theta_O(t)=\exp\left[-\int_0^t IA(t)dt\right], \quad (1)$$

where $A(\tau)=A_0R(\tau)^2$ is the area of the islands with "radius" $R(\tau)$ [30], and $dR(\tau)/d\tau=v(\tau)$. Thus, for the standard Avrami model with circular islands, one has that $A(\tau)=\pi v^2\tau^2$.

3.3. Simulation predictions and experimental results for oxygen uptake kinetics

We now demonstrate that our own model can also reproduce the desired form of the oxygen uptake curves, i.e., a transition from Langmuirian to sigmoidal forms with increasing temperature. Using E_{des}=3.4 eV and E_{con}=3.05 eV, simulation results displayed in Fig. 4 (Top) predict Langmuirian type behavior at low temperatures (up to around 580 °C) and a clear transition to a sigmoidal mode at higher temperatures starting at around 600 °C for a fixed O pressure of 2×10^{-7} Torr. Indeed, the behavior exhibited by these uptake curves differs only slightly from experiment shown in Fig. 4 (Bottom), where operating conditions are similar. However, in the experiment, uptake curves remain Langmuirian in form until 600 °C instead of 580 °C for the above choice of model parameters.

Additional analysis was performed exploring the effect of varying parameters such as E_{des} and E_{con} on the behavior of uptake curves at 600 °C and oxygen pressure of 2×10^{-7} Torr. We found that these curves show great sensitivity to both parameters. In Fig. 5 (Top), we notice an unmistakable shift towards a sigmoidal form with decreasing E_{des}. However, this shift can be countered by lowering E_{con}, as the resulting higher conversion rate from OS to BB (and BB to OS) results in more oxide islands nucleating early and causing the oxygen buildup to accelerate. Fig. 5 (Bottom) shows that curves progressively become more Langmuirian in shape with decreasing E_{con}.

It is appropriate to assess whether one can counterbalance these contrasting effects by simultaneously increasing E_{des} and E_{con} to achieve an uptake curve qualitatively similar to that generated using standard choice of parameters (i.e, E_{des}=3.5 eV and E_{con}=3.04 eV). We find that this strategy is somewhat effective for modest deviations from the standard values. For example, upon simultaneously increasing E_{des} to 3.6 eV and E_{con} to 3.15 eV, the resulting curve nearly overlaps with the reference curve for most of the process. However, we do find that the initial uptake behavior is

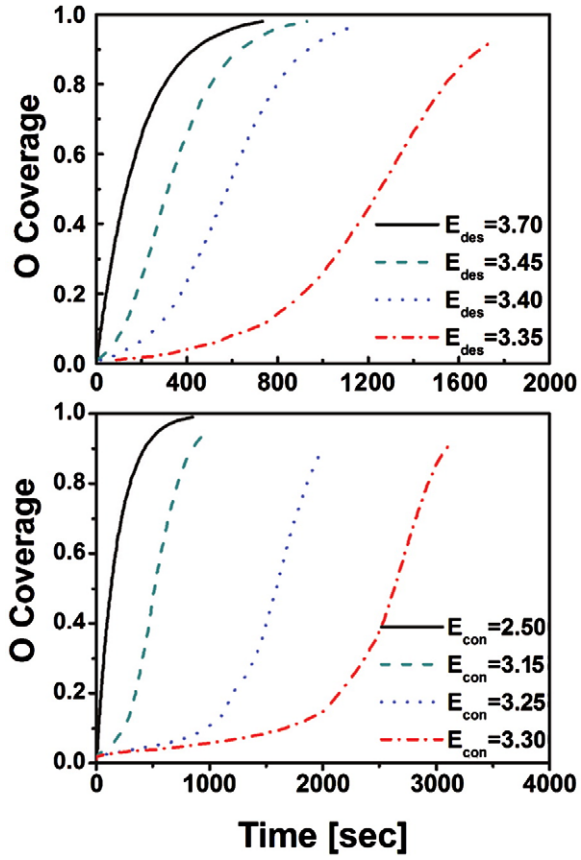

Fig. 5. *(Top)* Oxygen uptake curves at 600 °C and 2×10^{-7} Torr for E_{des}=3.70, 3.45, 3.4, and 3.35 eV (left to right). *(Bottom)* Oxygen uptake curves at 600 °C and 2×10^{-7} Torr for E_{con}=2.5, 3.15, 3.25, and 3.3 eV (left to right).

distinct. The slower desorption rate for the modified parameters means that initially there is a more rapid buildup of OS oxygen. In addition, the delayed onset of OS to BB (and BB to OS) conversion due to higher E_{con} creates a bottleneck to oxide formation which ensures that most of the adsorbed oxygen is in the form of OS and thus available for desorption, a process that soon eases the initial build-up of coverage. Other parameters of relevance that could potentially affect the shape of the uptake curve, namely E_O, and c_1 are similarly tested. It was found that the impact of c_1 on uptake is not as substantial as E_{des} and E_{con}. Furthermore, the effect of E_O is only minimal thus leaving the uptake curves relatively unchanged for modest 0.1–0.2 eV increments in E_O.

A key conclusion of the above studies is that the trends in the experimentally observed uptake kinetics can be recovered by our simulation model, despite the feature that it is rather different from a simple ACR or "incomplete condensation" models. This should be kept in mind when interpreting experimental data with such models.

To motivate a more detailed interpretation and analysis of behavior in our model, we show in Fig. 6 the shapes of the oxide islands after sustained growth at 620 °C and F=0.0054 ML/s. These are either near-square or near-rectangular, thus containing very few kinks. This behavior can be anticipated from the observation that the conversion rate is 0.06 s^{-1} at sites along straight edges versus 31 s^{-1} at kinks (with rates evaluated at 620 °C). Thus, the nucleation rate to create a new layer along a straight edge of length L (in lattice constants) of a rectangular cluster is R_{nuc}=0.06 L s^{-1}. Provided L<20, this is less than the rate, R_{zip}~30/L s^{-1} to complete a new edge once it is nucleated by conversion at kink sites zipping along that edge. Thus, island growth is limited by edge nucleation in this regime, and the rate of expansion of island edges is roughly proportional to the edge length, as thus to the effective radius. Similar behavior has been analyzed for so-called cooperative sequential adsorption models [29]. Consequently the sigmoidal oxygen uptake might be regarded as following from a generalized Avrami model choosing $v(\tau)=dR/d\tau=a(c+R)$, where a and c are constants, so that $v(t)=cae^{at}$.

3.4. Simulation predictions and experimental results for oxide nucleation kinetics

Here, we compare experimental observations with KMC simulation data for the evolution of the density of oxide islands, N_{ox}, of three or more BB atoms as a function of the number of Si layers etched. The relevant experimental data is found in Ref. [6], where T=600 °C and O_2 pressure is 6×10^{-8} Torr. As in the case of O uptake curves, we investigated the sensitivity of the oxide island density to E_{des} and E_{con}. We thereby obtain specific combinations of these two

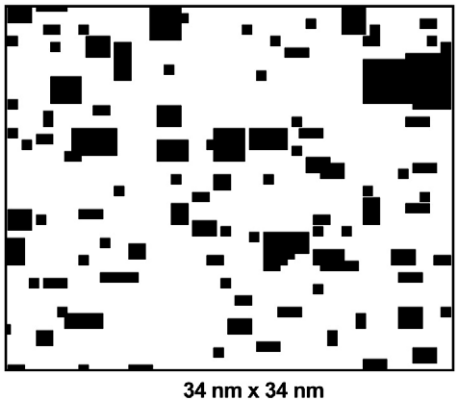

Fig. 6. Simulation results for an ensemble of oxide islands at 620 °C with F=0.0054 ML/s. Area: 34 nm×34 nm.

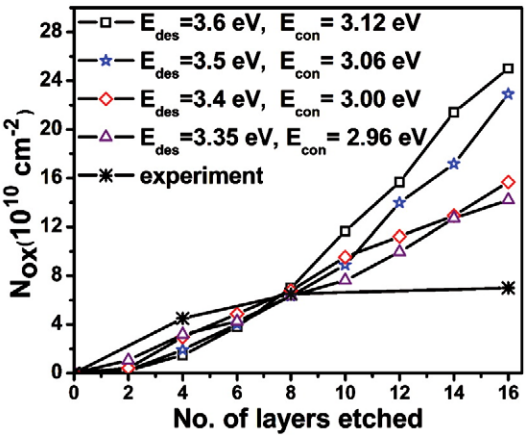

Fig. 7. Oxide cluster density, N_{ox}, vs. number of layers etched at T=600 °C. Experimental data is obtained from Ref. [6].

parameters which result in agreement between KMC simulations and experiment after 8 layers etched. In this analysis, we keep all other parameters fixed. However, we must choose a low value of ν_{con}~$10^{13.5}$ s^{-1} in order to match experimental oxide density for 8 layers etched with a choice of E_{con} of 3.06 eV close to our standard selection. This does reflect a limitation of the current model, perhaps deriving from inadequacies of the input parameters obtained from previous studies or perhaps reflecting an over-simplified treatment of oxide island nucleation. From Fig. 7, it is clear that simultaneously increasing (or decreasing) both E_{des} and E_{con} can preserve the value of N_{ox} at 8 layers etched. This is not surprising since increasing E_{des} makes nucleation easier, and increasing E_{con} makes nucleation more difficult. Here, we should point out that degree of saturation in N_{ox} observed in the experiments after etching ~8 ML was not reproduced well in the simulations. Moreover, it is also evident from the plot that using somewhat lower values for E_{des} and E_{con} better mimics the initial steep rise seen in the experimental curve. Thus, our oxide island density analysis seems to favor lower E_{des}, perhaps restricting it to no more than 3.5 eV.

Finally, we offer one possible reason for why the experimentally observed N_{ox}-saturation is not fully recovered in the model. Although we have used a value for the oxygen diffusion barrier suggested by DFT studies, other previous works [2,11] have suggested that this barrier could be significantly lower. We now argue that an appropriately lower diffusion barrier could enhance saturation of N_{ox}. A key related quantity is the oxygen diffusion length, $L_{diff}=(h_O\tau_{des})^{1/2}$, before desorption as SiO. In the terminology of our model, h_O is the OS oxygen hop rate, and $\tau_{des}=1/h_{des}$ is OS oxygen lifetime before desorption, i.e., the inverse of the SiO desorption rate. (During diffusion over a distance L_{diff}, the O will convert between OS and BB states many times. However, if desorption from the BB state is inhibited, then the above simple analysis of L_{diff} still applies.) Next, consider the evolution of the mean oxide island separation, $L_{isl}=N_{ox}^{1/2}$ during prolonged exposure of the surface to oxygen. Initially, L_{isl} is far larger than L_{diff}, so that deposited oxygen cannot easily reach existing oxide islands, and thus potentially nucleates new islands or desorbs. However, continued nucleation of new oxide islands reduces L_{isl} to the point where it becomes comparable to L_{diff}. Then, one expects most deposited oxygen to diffuse to and aggregate with existing oxide islands rather than nucleate new islands, i.e., N_{ox} will saturate. At 600 °C , the observed L_{isl} is about 100 lattice constants at saturation. For L_{diff} to equal this value, a simple calculation using the prefactors in Table 1 reveals that the oxygen diffusion barrier E_O, must be at least 1.3 eV below E_{des}, i.e., that $E_O\leq$2.1 eV for E_{des}=3.4 eV.

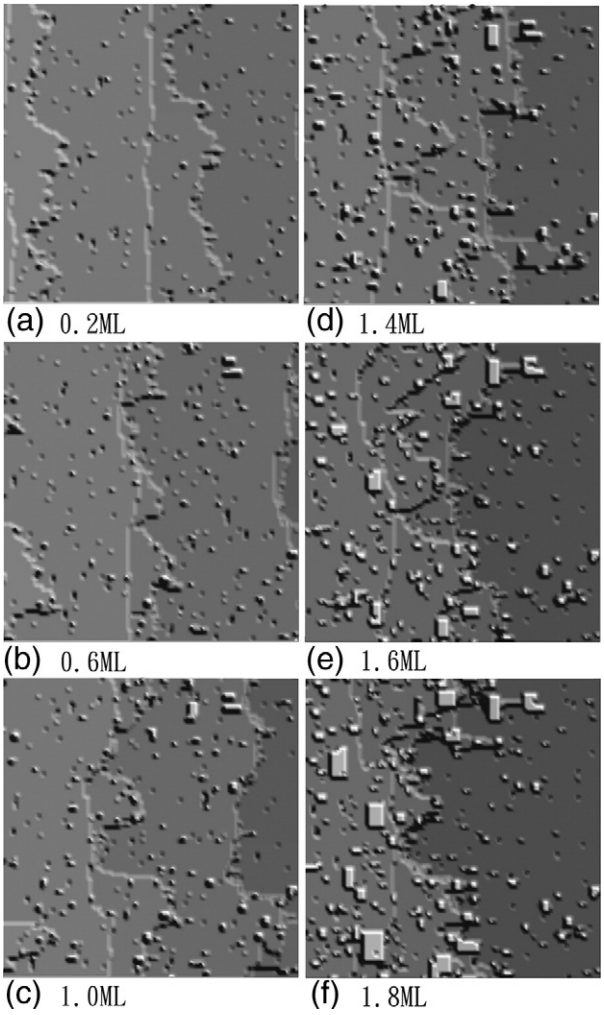

Fig. 8. A sequence of simulated images of vicinal Si(100) at different stages of etching (0.2 ML, 0.6 ML, 1.0 ML, 1.4 ML, 1.6 ML, and 1.8 ML) at 625 °C and 3.3×10^{-7} Torr. Oxide islands appear as brighter regions. Area: 70 nm×70 nm.

3.5. Modeling of competitive etching and oxidation on stepped surfaces: enhanced nucleation at steps

First, in Fig. 8, we present simulation images showing predictions of our full model, including Si(100) surface dynamics in addition to oxygen dynamics, for evolution of a stepped Si(100) surface during exposure to oxygen. We use the standard choice of parameters and choose T=625 °C and F=0.00891 ML/s, corresponding to $P_{O2}=3.3\times10^{-7}$ Torr. Initial step recession is apparent with meandering S_B steps catching up to straighter S_B steps, just as observed in experiment [1,5,6]. The di-vacancies, whose diffusion toward the step edges leads to this step recession, appear as dark spots in the images. After about 1.0 ML of the Si(100) surface has been etched, there is significant nucleation and growth of oxide islands (shown as the brighter regions in the image) for these conditions. The shapes of these oxide islands are reminiscent of those generated by the simpler model in Fig. 6 in which square or near-square islands tend to dominate.

Next, we modify our model to explore one of the most plausible reasons for enhanced nucleation at step edges – lowering of the nucleation barrier at S_B steps, a possibility raised by Brichzin et al. [11]. We chose not to modify behavior at S_A steps given a general consensus that S_B steps act as better traps for O atoms (compared to S_A steps or to the terrace). We compare simulation predictions for the dependence of oxide island density of surface miscut angle with the experimental data in Ref. [11] at a fixed O_2 exposure of 200 L (1 L=10^{-6} Torr s) during oxidation of Si(100) at O_2 pressure of 6×10^{-8} Torr and temperature T=690 °C. The miscut angle, θ, for the simulations is determined from the selected terrace width, w, by the relation $tan\theta=h/w$, where h=0.136 nm is the height of a surface step.

In our model, reduction in the nucleation barrier at steps corresponds to additional enhancement in the conversion rate of OS atoms into BB state but only if such atoms are adjacent to isolated BB atoms which are located at S_B steps. This will promote the formation of oxide islands at S_B steps. It is implemented in the model simply by increasing c_1 at steps by Δc_1. To satisfy detailed balance, the BB atoms resulting from such conversion can reconvert into OS at a rate commensurate to this extra enhancement, i.e., $E_{con}+(1-c_1-\Delta c_1)E_{ox}$.

Using Δc_1=0.19, one observes a general increase in the simulated density of oxide islands of two or more BB atoms from a value of 0.79×10^{10} cm^{-2} at ~0.2° (which is close to the experimental result of around 0.8×10^{10} cm^{-2}) to 1.68×10^{10} cm^{-2} at ~2.5°. The latter is close to the experimental value of 1.66×10^{10} cm^{-2} at a slightly higher miscut angle of 2.6°. This result explicitly demonstrates the viability of the aforementioned mechanism in boosting nucleation at step edges and mirrors the specific findings by Brichzin et al. [11].

3.6. Effectiveness of small oxide islands on step pinning

In this section, we explore the propensity for oxide islands to pin receding steps during oxidation of vicinal Si(100) leading to the emergence of finger-like step structures. Certainly, if oxide islands grow rapidly, they should have a strong propensity for pinning independent of their initial shapes. This is presumably the case at lower temperatures as applies in studies of Pelz et al. [1,4,5]. However, it is less clear whether small oxide islands typically formed at higher temperatures can effectively pin steps, and whether certain attributes of the islands might potentially be a factor in stabilizing the resulting fingers against pinch-off. Below we explore this issue and the possible impact of initial shape at the higher temperature of T=675 °C relevant for studies of Skrobiszewski et al. [31,32].

To provide a controlled assessment of the possible influence of oxide island shape (2D versus linear) on step pinning, it is convenient to introduce suitably distributed islands "by hand" on a vicinal surface at the beginning of the simulation. The evolution of these clusters will not be constrained, i.e., they can grow or shrink. Simulations of step pinning necessarily utilize our "full" model including Si(100) surface dynamics (rather than the simplified model). But, in order for our results to be physically relevant, we need to ensure that oxide islands can in fact form spontaneously in the temperature regime under consideration here. This feature is confirmed at T=675 °C and $P_{O2}=3.3\times10^{-7}$ Torr via efficient simulations using the simplified model which also reveal that such islands do not easily decay or shrink. The persistence of such small stable clusters plausibly applies in studies by Skrobiszewski et al. [31,32] where oxide clusters were not clearly visible in STM, but significant step pinning was observed.

Thus, in our simulations, we first place linear oxide islands of 4 BB atoms (which appear as small bright spots in Fig. 9) at periodic locations along S_B step edges in an otherwise clean vicinal Si(100) surface, then allow the surface to etch. The simulated surface morphologies at O_2 pressure of 3.3×10^{-7} Torr and temperature T=675 °C showing the oxide islands and the eroded step structures at various degrees of etching (0.4, 0.6 and 0.8 ML) are shown in Fig. 9(a)–(c). We then repeat these simulations placing square 2×2 BB atom oxide islands (rather than linear islands) along the S_B step edges at the start of the simulation. The resulting surface morphologies showing various degrees of etching are similarly displayed in Fig. 9(d)–(f).

Side by side comparisons of both cases reveal qualitatively similar morphologies up to about 0.4 ML etched. However, by about 0.6 ML, well-defined periodic arrays of V-shapes fingers develop at S_B steps from pinning by linear oxide islands on the left, but such features are

not so evident for 2D islands on the right. In contrast, pinch-off seems to be more prevalent for the 2D islands, as compared with linear islands containing the same number of atoms. (By pinch-off, we mean a process wherein the tips of fingers break off creating small Si islands, partly covered with oxide, which are separated from the rest of the receding step edge.) Furthermore, the former V-shaped morphologies appear most similar to those observed by Skrobiszewski et al. [31,32] also shown in Fig. 9g [33]. Why are linear oxide islands more effective in preventing pinch-off? In this case, a longer stretch of the step edge is protected by the island from etching by DV's diffusing from the upper terrace, thus the initial finger formed is wider and less susceptible to pinch-off. Finally, we should comment that fingers in the simulations are created primarily by S_B steps with low stiffness bending dramatically around oxide islands. By contrast, high stiffness S_A steps quickly pinch-off upon reaching these oxide islands. These features are also apparent in experiment.

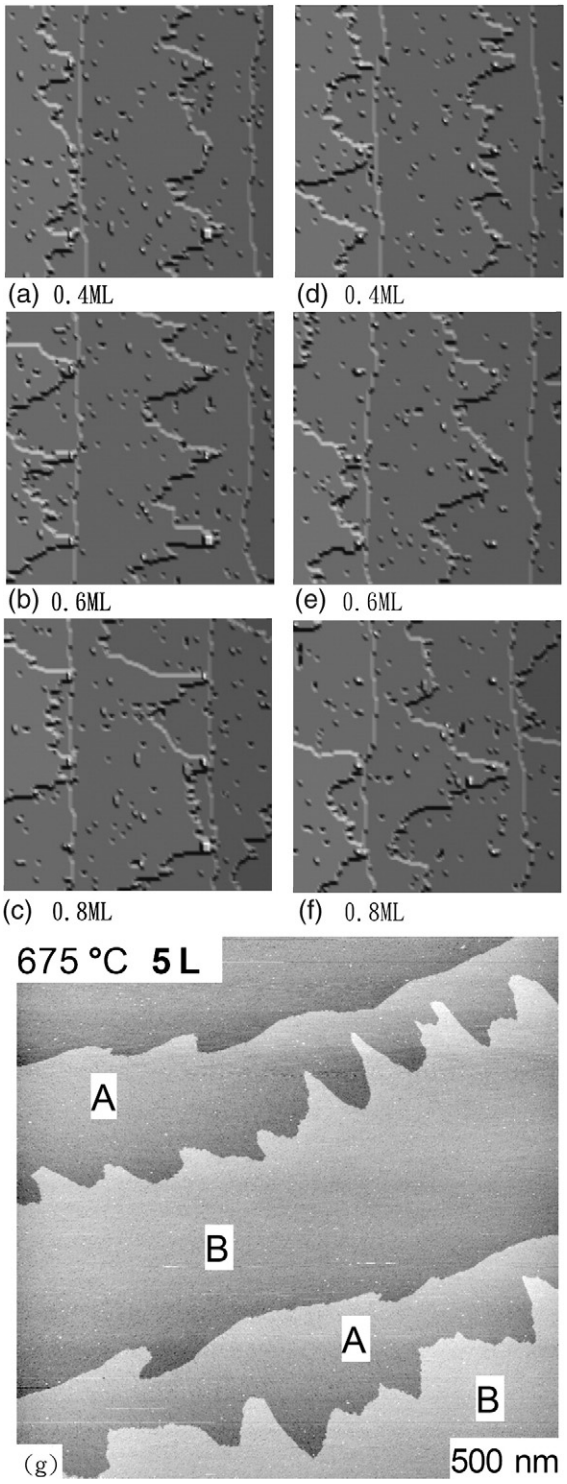

Fig. 9. (a–f) A sequence of simulated images of vicinal Si(100) at different stages of etching (0.4 ML, 0.6 ML, and 0.8 ML) 675 °C and 3.3×10^{-7} Torr. Images on the upper left (right) show surface evolution for three linear oxide islands (2D oxide islands) placed initially periodically along each rough S_B steps. Area: 70 nm×70 nm. (g) STM image from Ref. [31] showing V-shaped arrays of fingers formed during O_2 deposition at 675 °C and 3.3×10^{-7} Torr. Area: 500 nm×500 nm.

4. Conclusions

We have developed a lattice-gas model for etching and oxidation of Si(100) surfaces incorporating a recently observed transformation in initial oxide island shape from linear to two-dimensional. We show that this model with realistic energetic parameters can describe experimental observations on these initial island shape transitions, as well as oxygen uptake behavior, and surface morphologies produced during prolonged etching of vicinal surfaces. Modified parameters are needed to recover observed oxide island densities indicating some limitations of the current modeling. In addition, we use the new model to explore enhanced nucleation of oxide islands at steps, and to assess the propensity for small oxide islands to pin steps at higher temperature. We find that the initial linear island shape enhances pinning capability and produces morphologies similar to those observed in experiments of Skrobiszewski et al. [31,32].

Acknowledgment

This work was supported by the NCTS and the National Science Council of Taiwan under Grant No. NSC95-2112-M110-022. We are grateful to the National Center for High-performance Computing in Taiwan for computer time and facilities. JWE was supported by the US Department of Energy, Office of Basic Energy Sciences, through the Chemical Physics and SciDAC Computational Chemistry Programs. His work was performed at Ames Laboratory – USDOE which is operated by Iowa State University under Contract No. DE-AC02-07CH11358.

Appendix A. Island nucleation kinetics

Due to the complexity of our island nucleation and growth model, a precise analytic treatment is difficult. However, several of the key ingredients of this model appear in other simpler models, and it is appropriate to discuss these here. A so-called "$i=0$" model has been considered for heteroepitaxy involving nucleation via irreversible exchange of single diffusing adatoms with the substrate [34,35]. However, this is significantly different from our model where exchange is strongly reversible and nucleation requires a pair of OS and BB oxygen adatoms. In models for incomplete condensation, a key parameter is the diffusion length, L_{diff} before desorption. Desorption only impacts island formation in the regime where $L_{diff}<L_{isl}$ (the mean island separation) [22]. One has that $L_{diff}=11$ versus $L_{isl}=8$ (in lattice constants) in our model at 620 °C. Finally, we mention studies of attachment-limited island formation where there is a significant barrier for attachment of diffusing atoms and thus for island growth [34]. This might be regarded as the situation for our model where the barrier for exchange at straight island edges of $E_{con}=3.05$ eV far exceeds the OS oxygen hopping barrier of $E_O=2.4$ eV (where both processes are assigned the same prefactor). Denoting the barrier difference by $\delta E=0.6$ eV, it is useful to assign an attachment length $L_{attach}=\exp[-dE/(kT)]-1$. Since $L_{attach}=10^{3.7}$ far exceeds L_{isl} in our model at 620 °C, island growth is attachment rather than diffusion limited.

References

[1] C. Ebner, J.V. Seiple, J.P. Pelz, Phys. Rev., B 52 (1995) 16651.
[2] M.A. Albao, D.-J. Liu, C.H. Choi, M.S. Gordon, J.W. Evans, Surf. Sci. 555 (2004) 51.
[3] M.A. Albao, D-J. Liu, M.S. Gordon, J.W. Evans, Phys. Rev., B 72 (2005) 195420.
[4] J.V. Seiple, J.P. Pelz, Phys. Rev. Lett. 73 (1994) 999.
[5] J.V. Seiple, J.P. Pelz, J. Vac. Sci. Technol., A 13 (1995) 772.
[6] J.V. Seiple, C. Ebner, J.P. Pelz, Phys. Rev., B 53 (1996) 15432.
[7] H. Togashi, H. Asaoka, T. Yamazaki, M. Suemitsu, Jpn. J. App. Phys. 44 (2005) L1377.
[8] M. Udegawa, M. Sumita, I. Sumita, Jpn. J. App. Phys. 32 (1993) 283.
[9] K. Kato and, T. Uda, Phys. Rev., B 62 (2000) 15978.
[10] C.H. Choi, D.-J. Liu, J.W. Evans, M.S. Gordon, J. Am. Chem. Soc. 124 (2002) 8730.
[11] V. Brichzin, J.P. Pelz, Phys. Rev., B 59 (1999) 10138.
[12] Y. Wei, R.M. Wallace, A.C. Seabaugh, J. Appl. Phys. 81 (1997) 6415.
[13] A.M. Mazzone, Eur. Phys. J., B 35 (2003) 125.
[14] D.J. Chadi, Phys. Rev. Lett. 43 (1987) 43.
[15] M. Suemitsu, Y. Enta, Y. Miyanishi, N. Miyamoto, Phys. Rev. Lett. 82 (1999) 2334.
[16] A. Esteve, Y.J. Chabal, K. Raghavachari, M.K. Weldon, K.T. Queeney, M. Djafari Rouhani, J. Appl. Phys. 90 (2001) 6000.
[17] A.B. Bortz, M.H. Kalos, J.L. Lebowitz, J. Comp. Phys. 17 (1975) 10.
[18] T. Uchiyama, T. Uda, K. Terakura, Surf. Sci. 474 (2001) 21.
[19] J.R. Engstrom, D.J. Bonser, M.M. Nelson, T. Engel, Surf. Sci. 256 (1991) 317.
[20] D.-J. Liu, C.H. Choi, M.S. Gordon, J.W. Evans, MRS Proc. 619 (2000) 179.
[21] H. Togashi, Y. Enta, M. Suemitsu, Appl. Surf. Sci. 252 (2006) 5900.
[22] J.W. Evans, P.A. Thiel, M.C. Bartelt, Surf. Sci. Rep. 61 (2006) 1.
[23] P. Jensen, H. Larralde, A. Pimpinelli, Phys. Rev., B 55 (1997) 2556.
[24] M. Avrami, J. Chem. Phys. 7 (1940) 1103.
[25] M. Avrami, J. Chem. Phys. 8 (1941) 212.
[26] M. Avrami, J. Chem. Phys. 9 (1942) 177.
[27] P.A. Mulheran, D.A. Robbie, Philos. Mag. Lett. 78 (1998) 247.
[28] S. Ohta, T. Ohta, K. Kawasaki, Physica A 140 (1987) 478.
[29] J.W. Evans, Rev. Mod. Phys. 65 (1993) 1281.
[30] For non-circular islands, R can be regarded as the average linear dimension over all possible directions. For square islands, R is of the order of half the length of a side.
[31] J.L. Skrobiszewski, Masters Thesis, Virginia Commonwealth University, USA, 2003.
[32] J.L. Skrobiszewski, J.C. Moore, J.W. Dickenson, A.A. Baski, J. Vac. Sci. Technol., A 22 (2004) 1667.
[33] Comparing the KMC simulation images (70 *nm*×70 *nm*) and STM image (500 *nm*×500 *nm*) in Fig. 9, we should note that the difference in scale implies a significantly higher density of fingers in the simulation images. However, recall that the oxide islands were inserted by hand in the simulation with an articicially high density in order to show arrays of fingers in our smaller simulation cell. It is however surprising that the fingers form a such a regular array in the experiment, as one expects more random nucleation locations in the simulation.
[34] D. Kandel, Phys. Rev. Lett. 78 (1997) 499.
[35] A. Zangwill, E. Kaxiras, Surf. Sci. 32 (1995) L483.